



# DESIGN AND OPTIMIZATION OF LATTICE STRUCTURES FOR AEROSPACE APPLICATIONS

Enrico Stragiotti

François-Xavier Irisarri<sup>1</sup>, Cédric Julien<sup>1</sup> and Joseph Morlier<sup>2</sup>

1: ONERA - The French Aerospace Lab  
DMAS - Département matériaux et structures  
92320 Châtillon, France  
[{francois-xavier.irisarri, cedric.julien}@onera.fr](mailto:{francois-xavier.irisarri, cedric.julien}@onera.fr)

2: ICA - Institut Clément Ader  
ISAE - SUPAERO  
31400 Toulouse, France  
[joseph.morlier@isae-supraero.fr](mailto:joseph.morlier@isae-supraero.fr)  
January 22, 2024

PhD manuscript

ONERA – ISAE Supaero

## **Colophon**

This document was typeset with the help of KOMA-Script and L<sup>A</sup>T<sub>E</sub>X using the kaobook class.

ONERA – ISAE Supaero

# CONTENTS

<b>Contents</b>	<b>iii</b>
<b>List of Figures</b>	<b>v</b>
<b>List of Tables</b>	<b>v</b>
<b>List of Abbreviations</b>	<b>v</b>
<b>1 Design of real-size aeronautical wing structures</b>	<b>1</b>
1.1 3D CRM wingbox with multiple load cases . . . . .	1
1.1.1 Advanced thresholding . . . . .	2
1.1.2 Numerical application . . . . .	2
1.2 NACA profile extruded . . . . .	9
1.2.1 Numerical implementation . . . . .	9
1.2.2 Meshing irregular volumes . . . . .	9
1.2.3 Definition of the repetitive zones . . . . .	9
1.2.4 Numerical application . . . . .	9
1.3 Conclusion . . . . .	9
<b>Bibliography</b>	<b>11</b>



## LIST OF FIGURES

1.1	(a) Ground structure of the CRM-315 test case; (b) Ground structure of the CRM-2370 test case. The cross-sectional areas shown in the two sub-figures represent the starting point of the optimizations. . . . .	3
1.2	Optimized topology of the CRM-315 with 257 active bars. . . . .	3
1.3	Maximum stress constraint value (left) and buckling constraint value (right) plotted on the deformed shape of the optimized design (undeformed shape in light grey) of CRM-2370 for the three load cases: +2.5 g maneuver (a), -1 g maneuver (b), and cruise with gust (+1.3 g) (c). The maximum z tip deflection is 4.167 m, -2.953 m, and 1.948 m, respectively. . . . .	6
1.4	Normalized buckling and maximum stress constraint values for the optimized CRM-2370 structure after the SLP and the NLP optimization steps. . . . .	7
1.5	Iteration history of the CRM-315 example solved with the 2S-5R algorithm. (a) objective function history for the SLP and NLP step. The sharp increases in the objective function during the SLP step correspond to the reinitialization calls. (b) constraint violation for the NLP step. . . . .	7
1.6	Iteration history of the CRM-2370 example solved with the 2S-5R algorithm. (a) objective function history for the SLP and NLP step. The sharp increases in the objective function during the SLP step correspond to the reinitialization calls. (b) constraint violation for the NLP step. . . . .	8

## LIST OF TABLES

1.1	Material data used for the CRM optimization. . . . .	2
1.2	Numerical results of the optimization of the CRM with two different ground structures. . . . .	2
1.3	Number of active mechanical failure constraints for the CRM-2370 optimized design per type of constraint (rows) and per load case (columns). . . . .	5

## LIST OF ABBREVIATIONS

<b>CRM</b>	NASA Common Research Model
<b>FEA</b>	Finite Element Analysis
<b>MILO</b>	Mixed-Integer Linear Optimization
<b>NLP</b>	Non-Linear Programming
<b>SLP</b>	Sequential Linear Programming



## tables always small Introduction

Ultralight trusses are a good design candidate for the design of innovative aerostructures thanks to their superior aeroelastic properties and stiffness-to-weight ratio [1]. These structures represent a natural application case for the discussed optimization formulations. [2, 3] proposed a two-step sequential optimization algorithm to reduce the weight of a truss wing. Firstly, a ground structure with different nodal densities based on the stress field of the structure is generated and secondly, the cross-sectional areas are found using a sizing optimization algorithm that takes into account stress, local buckling, and aeroelastic constraints. [4] decided, instead, to tackle all the difficulties of the problem using a set of discrete cross-sectional areas and a sizing Mixed-Integer Linear Optimization (MIL) algorithm. The algorithm is validated on a 315-bars wingbox ground structure, based on the NASA Common Research Model (CRM). In these studies, the adoption of a sizing optimization algorithm simplifies the numerical complexities associated with the problem. However, by solely focusing on modifying the component sizes, the opportunity to optimize the overall truss topology is missed, limiting the potential for further weight savings.

## 1.1 3D CRM WINGBOX WITH MULTIPLE LOAD CASES

In this section, the proposed strategy is used to optimize a real-size wingbox, to validate its ability to work on large, three-dimensional structures with more candidate members compared to the precedent test cases. The structure is based on the jig (undeformed) shape of the wingbox of the NASA CRM [5]. The structure is submitted to three different load cases: +2.5 g maneuver (LC\_1), -1 g maneuver (LC\_2), and cruise with gust +1.3 g (LC\_3). The nodes of the bounding volume and the loads used are provided by [6], where a detailed discussion on how they are evaluated can be found. The ground structure of the test case is presented in Fig. 1.1a.

The material used for the optimization is an aluminum alloy with Young's modulus of 69 GPa, density of 2.7 g/cm<sup>3</sup>, and yield stress equal to ±270 MPa (see Table 1.1). To ensure a conservative design, we incorporated safety factors (*sf*) associated with each load case. These safety factors were integrated into the formulation by reducing the maximum stress and buckling allowables by factors of 1.5, 1.5, and 2.67 for the three considered load cases, respectively. No bounds

1.1 3D CRM WINGBOX WITH MULTIPLE LOAD CASES . . . . .	1
1.2 NACA PROFILE EXTRUDED . . . . .	9
1.3 CONCLUSION . . . . .	9

- 1. Cramer et al. (2019), 'Elastic shape morphing of ultralight structures by programmable assembly'
- 2. Opgenoord et al. (2018), 'Aeroelastic Tailoring using Additively Manufactured Lattice Structures'
- 3. Opgenoord et al. (2019), 'Design for additive manufacturing: cellular structures in early-stage aerospace design'
- 4. Shahabsafa et al. (2018), 'A novel approach to discrete truss design problems using mixed integer neighborhood search'

5. Brooks et al. (2018), 'Benchmark Aerostructural Models for the Study of Transonic Aircraft Wings'

6. Fakhimi et al. (2021), 'Discrete multi-load truss sizing optimization'

constraints are imposed on the nodal displacements of the structure and the cross-sections are assumed circular with the cross-sectional buckling parameter  $s = \pi E/4$ . The optimization is carried only on the wingbox, the internal structure of the wing, and there is no influence of the skin on the optimization.

Parameter	Value
$E$	69 GPa
$\sigma_c, \sigma_t$	$\pm 270$ MPa
$\rho$	$2.7 \text{ g cm}^{-3}$

**Table 1.1:** Material data used for the CRM optimization.

Equation ?? reads:

$$a_i < a_{\text{thr}} \quad \forall i, \text{ with } a_{\text{thr}} = \chi \max(\tilde{a}^*)$$

### 1.1.1 ADVANCED THRESHOLDING

As the CRM is a large and thin structure that presents a noticeable difference in load magnitude between the tip and the root of the wingbox, the quantities of interest of the optimization span different orders of magnitude (from  $\text{m}^2$  to  $\text{mm}^2$ , and from MN to N). For that reason, the choice of the cross-sectional area threshold value  $\chi$  defined in Equation ?? and used to simplify the initial Non-Linear Programming (NLP) ground structure is crucial. Taking a high value (such as  $\chi = 10^{-4}$ , restraining the solution from  $\text{m}^2$  to  $\text{cm}^2$ ) would mean possibly canceling out bars fundamental for the nodal force equilibrium in the less loaded part of the wing (wing tip and the central part of the wing's sections near the root). By contrast, a low value (such as  $\chi = 10^{-9}$ ) would permit the correct simulation of the mechanical response of the structure, but it would lead to a very high number of candidate bars and, thus, longer optimizations and convergence difficulty for the NLP phase. For that reason,  $\chi$  is set to an average value ( $\chi = 10^{-6}$ ), eliminating all the bars under the value  $a_{\text{thr}} = \chi \max(a)$ , but an additional check is performed before proceeding to the thresholding. The bars under the threshold  $a_{\text{thr}}$  are sorted in ascending order of cross-sectional area and, starting from the smallest one, we iteratively check via a Finite Element Analysis (FEA) that the difference between the force and displacement fields before and after the bar removal is below than a certain bound. In the present study we used the following:  $\|\Delta q\|_\infty < 10 \text{ N}$  and  $\|\Delta U\|_\infty < 1 \text{ cm}$ .

### 1.1.2 NUMERICAL APPLICATION

Two different discretizations are considered for the optimization. The proposed algorithm is firstly tested on the same ground structure provided by Fakhimi *et al.* [6], composed of  $N_{\text{el}} = 315$  candidate

6. Fakhimi et al. (2021), 'Discrete multi-load truss sizing optimization'

**Table 1.2:** Numerical results of the optimization of the CRM with two different ground structures.

Quantity	CRM-315	CRM-2370
$N_{\text{el}}$	315	2370
$N_{\text{opt}}$	257	1127
$V [\text{m}^3]$	7.90	7.44
$V [\%]$	1.309 %	1.232 %
Mass [t]	21.342	20.092
$a_{\text{max}} [\text{m}^2]$	0.198	0.208
$C_{\text{LC\_1}} [\text{MJ}]$	3.23	3.17
$C_{\text{LC\_2}} [\text{MJ}]$	1.28	1.27
$C_{\text{LC\_3}} [\text{MJ}]$	0.76	0.74
$t [\text{s}]$	147	3189

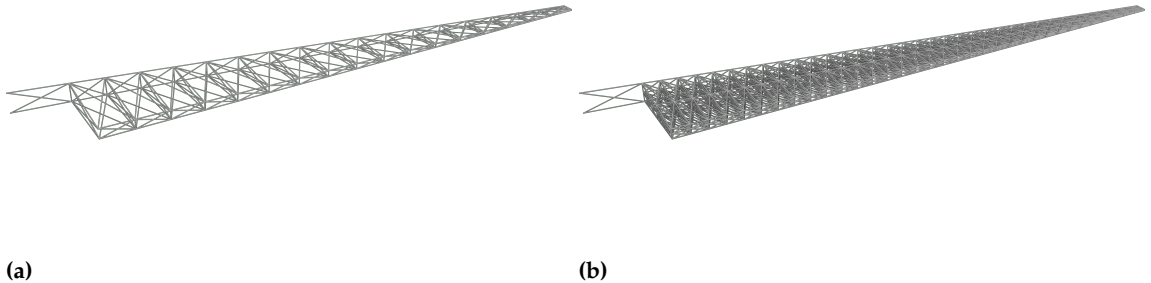


**Figure 1.1:** (a) Ground structure of the CRM-315 test case; (b) Ground structure of the CRM-2370 test case. The cross-sectional areas shown in the two sub-figures represent the starting point of the optimizations.



**Figure 1.2:** Optimized topology of the CRM-315 with 257 active bars.

members (CRM-315). The second discretization is obtained by refining the 315-bar ground structure, evaluating the midpoints of every member, and connecting them with first-order connectivity. We obtain  $N_{el} = 2370$  candidate members (CRM-2370). The loads and the boundary conditions are applied on the same nodes of the ground structure for the two studied ground structures. The cross-sectional areas of the starting point of the CRM-315 and the CRM-2370 are set to  $0.0001 \text{ m}^2$  and they are shown in Fig. 1.1. Only one single start point is used for these two examples as the proposed two-step strategy with reinitialization already proved in the previous sections to reduce the starting point influence on the optimization result. The resolution algorithm used is 2S-5R. The numerical results of the optimization for the two different discretizations are reported in Table 1.2.

The optimized CRM-315 structure shows a mass of 21.342 t, a 27.01 % reduction compared to the solution with discrete cross-section areas found by Fakhimi *et al.* [6] (29.238 t). Other than the substantial difference in the modelization of the cross-section areas, the mass reduction could be explained by the fact that the proposed algorithm has a zero lower bound on cross-sectional areas, thus permitting the topology of the structure to change: the 2S-5R solution shows 257 active bars out of 315 at convergence (see Fig. 1.2). In contrast, the MILO problem solved by Fakhimi *et al.* [6] is employed as a sizing optimization algorithm with fixed topology (and thus 315 active members in the optimized design). A more detailed comparison could not be performed as the authors did not share the values of the cross-sectional areas of their solution.

6. Fakhimi et al. (2021), 'Discrete multi-load truss sizing optimization'

The volume fraction of the solution is 1.313 % and the minimum slenderness ratio  $\lambda$  (ratio between the length and the radius of gyration of the bar) of a bar is 14.96, which is compatible with the truss modelization used to discretize the wingbox volume. The execution time of the optimization is 19 s for the Sequential Linear Programming (SLP) step and 128 s for the NLP step, for a total of 147 s on a regular notebook, compared to the over four days of optimization of Fakhimi [6] on a desktop workstation. The iteration history curves of the optimization are plot in Fig. 1.5.

#### MAXIMUM DISPLACEMENTS CONSTRAINTS

**MULTIPLE MATERIALS** complete with Ashby charts on cost and co2 evaluation

**ENRICHING THE MESH** The mass of the optimized CRM-2370 structure is 20.092 t, a 1.318 t reduction compared to the CRM-315 (-6.2 %). Additionally, if we compare the compliance of the three load cases (see Table 1.2), we notice how the solution of CRM-2370 is not only lighter but also stiffer, suggesting in general a more efficient structure topology. The maximum z tip deflection of the wingbox is 4.167 m, -2.953 m, 1.948 m for the three considered load cases, respectively. There are 1127 active bars in the optimized design, and the whole optimization took 3189 s (1911 s for the SLP step, 1278 s for the NLP step). The iteration history curves of the optimization are plot in Fig. 1.6. In Fig. 1.3 the normalized maximum stress and buckling constraints are plotted on the deformed shape of the three load cases. We notice how in general the topology of the two external "spars" is shaped after the +2.5 g load case, while the interior of the wingbox is made by a thinner truss constrained by buckling.

**ACTIVE MECHANICAL CONSTRAINTS** To better understand which mechanical phenomena is the most constraining for the bars of the solution, we present in Fig. 1.4 a graph where the normalized stress criterion  $c_s = \max(-q sf/\sigma_c a, q sf/\sigma_t a)$  and the normalized buckling criterion  $c_b = q sf/q_{crit}$  are plotted against each other. Every point in the scatter plot represents the members of the solution of the SLP and the NLP steps that show at least a charge of 1N (931 out of 1127 members). This threshold is applied as at the end of the NLP step some members present a very small section, creating numerical problems when evaluating the stress and buckling criteria. All the SLP members activate either the maximum stress or buckling limit, while 68 out of 931 NLP members are located in the center of the graph ( $c_s < 0.95$  and  $c_b < 0.95$ ). We speculate that this behavior is due to the inclusion of the kinematic compatibility constraint in the

	<b>LC_1</b>	<b>LC_2</b>	<b>LC_3</b>	<b>Tot.</b>
<b>Buckling</b>	281	145	143	569
<b>Tension</b>	56	3	4	63
<b>Compression</b>	286	6	6	298
<b>Tot.</b>	623	154	153	930

**Table 1.3:** Number of active mechanical failure constraints for the CRM-2370 optimized design per type of constraint (rows) and per load case (columns).

NLP algorithm: the cross-sectional area of these bars is chosen to comply with the global displacements. In Table 1.3, a summary of the active mechanical failure constraints (buckling, tensile stress, and compressive stress) present in the NLP solution. The table showcases the number of active constraints categorized by constraint type and load case. The optimized design encompasses a total of 930 active mechanical failure constraints for 863 bars (931 minus the 68 bars constrained by kinematic compatibility). This suggests that certain members are concurrently subject to multiple failure constraints across different load cases. An additional observation is that the design of the solution is primarily influenced by local buckling and compressive failures, especially under the +2.5 g load case (LC\_1).

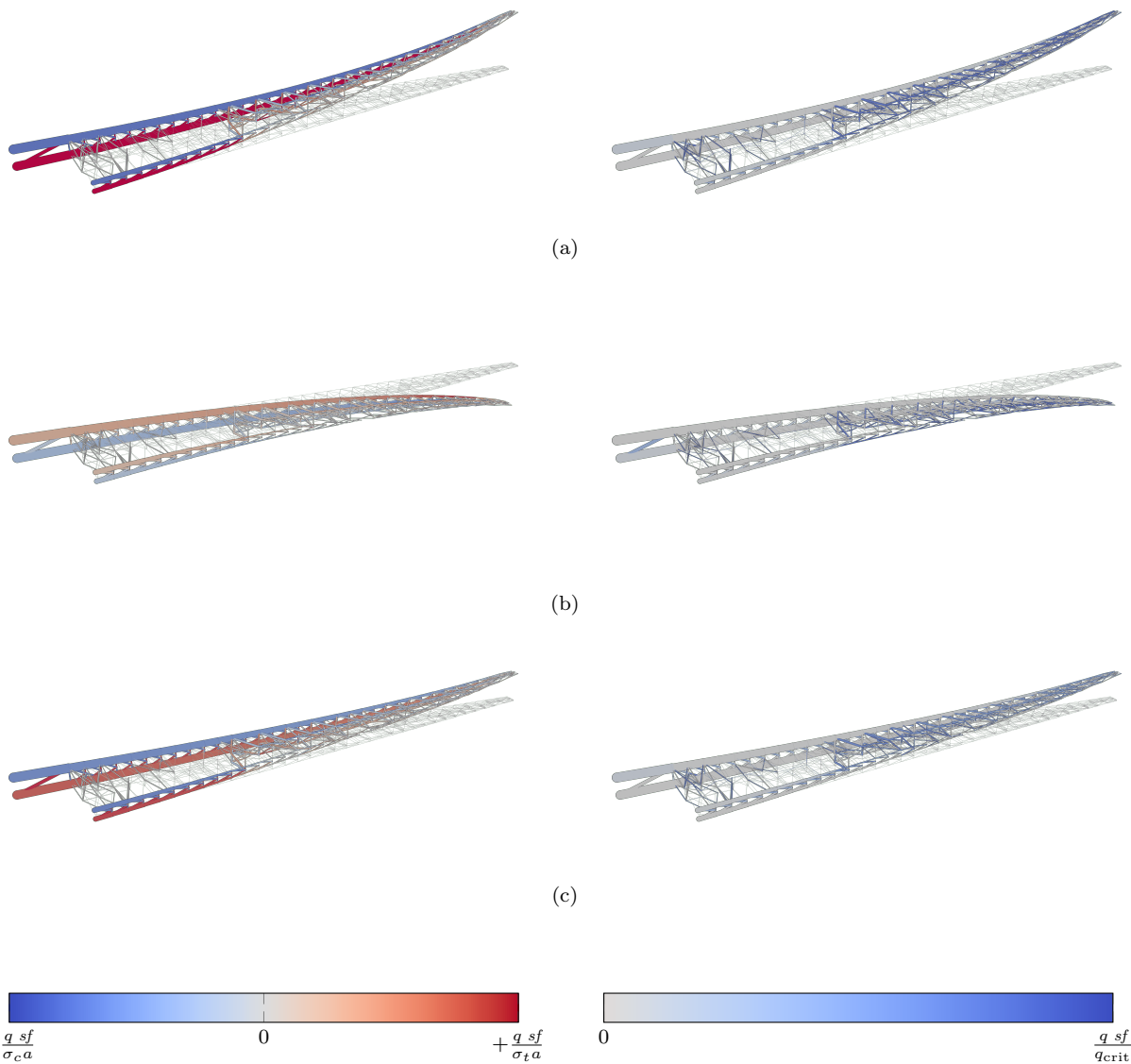


**Figure 1.3:** Maximum stress constraint value (left) and buckling constraint value (right) plotted on the deformed shape of the optimized design (undeformed shape in light grey) of CRM-2370 for the three load cases: +2.5 g maneuver (a), -1 g maneuver (b), and cruise with gust (+1.3 g) (c). The maximum  $z$  tip deflection is 4.167 m, -2.953 m, and 1.948 m, respectively.

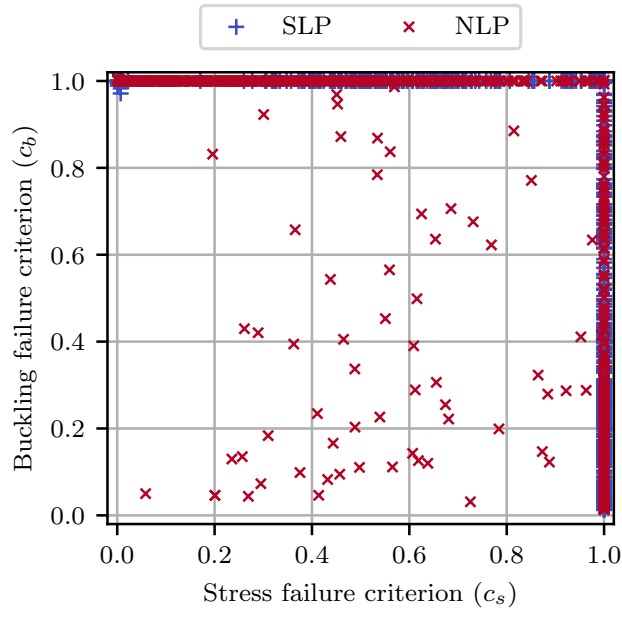


**Figure 1.4:** Normalized buckling and maximum stress constraint values for the optimized CRM-2370 structure after the SLP and the NLP optimization steps.

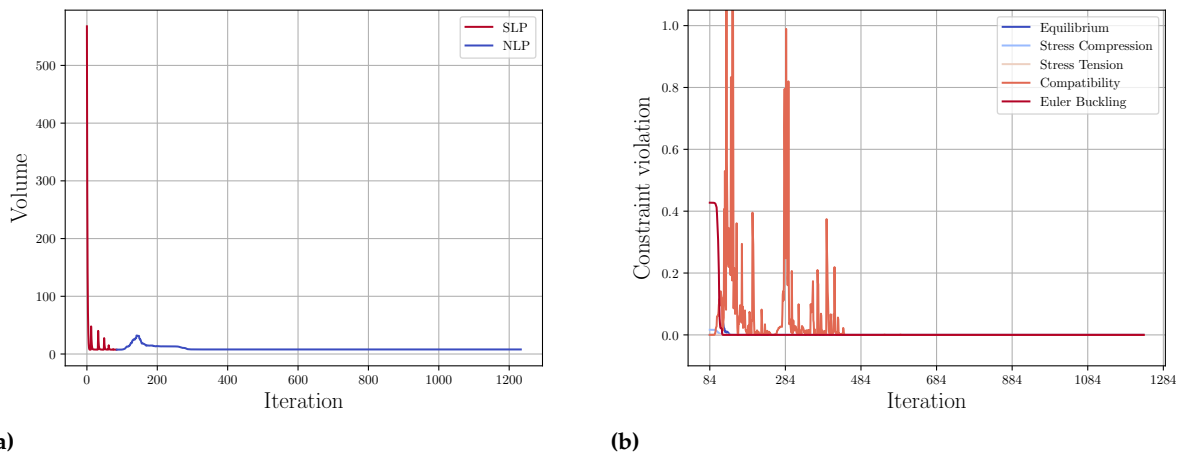


**Figure 1.5:** Iteration history of the CRM-315 example solved with the 2S-5R algorithm. (a) objective function history for the SLP and NLP step. The sharp increases in the objective function during the SLP step correspond to the reinitialization calls. (b) constraint violation for the NLP step.

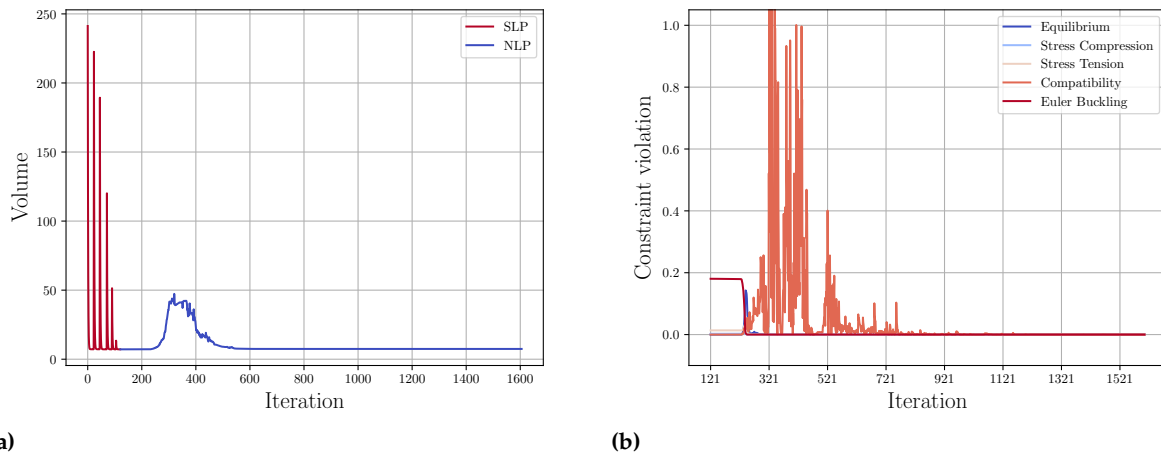


**Figure 1.6:** Iteration history of the CRM-2370 example solved with the 2S-5R algorithm. (a) objective function history for the SLP and NLP step. The sharp increases in the objective function during the SLP step correspond to the reinitialization calls. (b) constraint violation for the NLP step.

## 1.2 NACA PROFILE EXTRUDED

### 1.2.1 NUMERICAL IMPLEMENTATION

### 1.2.2 MESHING IRREGULAR VOLUMES

### 1.2.3 DEFINITION OF THE REPETITIVE ZONES

### 1.2.4 NUMERICAL APPLICATION

## 1.3 CONCLUSION



## BIBLIOGRAPHY

- [1] Cramer, N. B., Cellucci, D. W., Formoso, O. B., Gregg, C. E., Jenett, B. E., Kim, J. H., Lendraitis, M., Swei, S. S., Trinh, G. T., Trinh, K. V., and Cheung, K. C., 'Elastic shape morphing of ultralight structures by programmable assembly', *Smart Materials and Structures* 28.5 (Apr. 2019), p. 055006.  
doi: [10.1088/1361-665X/ab0ea2](https://doi.org/10.1088/1361-665X/ab0ea2) cited on page 1
- [2] Opgenoord, M. M. and Willcox, K. E., 'Aeroelastic Tailoring using Additively Manufactured Lattice Structures', *2018 Multi-disciplinary Analysis and Optimization Conference*, Atlanta, Georgia: American Institute of Aeronautics and Astronautics, June 2018.  
doi: [10.2514/6.2018-4055](https://doi.org/10.2514/6.2018-4055) cited on page 1
- [3] Opgenoord, M. M. J. and Willcox, K. E., 'Design for additive manufacturing: cellular structures in early-stage aerospace design', *Structural and Multidisciplinary Optimization* 60.2 (Aug. 2019), pp. 411–428.  
doi: [10.1007/s00158-019-02305-8](https://doi.org/10.1007/s00158-019-02305-8) cited on page 1
- [4] Shahabsafa, M., Mohammad-Nezhad, A., Terlaky, T., Zuluaga, L., He, S., Hwang, J. T., and Martins, J. R. R. A., 'A novel approach to discrete truss design problems using mixed integer neighborhood search', *Structural and Multidisciplinary Optimization* 58.6 (Dec. 2018), pp. 2411–2429.  
doi: [10.1007/s00158-018-2099-8](https://doi.org/10.1007/s00158-018-2099-8) cited on page 1
- [5] Brooks, T. R., Kenway, G. K. W., and Martins, J. R. R. A., 'Benchmark Aerostructural Models for the Study of Transonic Aircraft Wings', *AIAA Journal* 56.7 (July 2018), pp. 2840–2855.  
doi: [10.2514/1.J056603](https://doi.org/10.2514/1.J056603) cited on page 1
- [6] Fakhimi, R., Shahabsafa, M., Lei, W., He, S., Martins, J. R. R. A., Terlaky, T., and Zuluaga, L. F., 'Discrete multi-load truss sizing optimization: model analysis and computational experiments', *Optimization and Engineering* (Sept. 2021).  
doi: [10.1007/s11081-021-09672-6](https://doi.org/10.1007/s11081-021-09672-6) cited on pages 1–4

